
SELF-SUPERVISED JEPA-BASED WORLD MODELS FOR LiDAR OCCUPANCY COMPLETION AND FORECASTING

Haoran Zhu, Anna Choromanska

Department of Electrical and Computer Engineering
New York University
`{hz1922, ac5455}@nyu.edu`

ABSTRACT

Autonomous driving, as an agent operating in the physical world, requires the fundamental capability to build *world models* that capture how the environment evolves spatiotemporally in order to support long-term planning. At the same time, scalability demands learning such models in a self-supervised manner; *joint-embedding predictive architecture (JEPa)* enables learning world models via leveraging large volumes of unlabeled data without relying on expensive human annotations. In this paper, we propose **AD-LiST-JEPa**, a self-supervised world model for autonomous driving that predicts future spatiotemporal evolution from LiDAR data using a JEPa framework. We evaluate the quality of the learned representations through a downstream LiDAR-based occupancy completion and forecasting (OCF) task, which jointly assesses perception and prediction. Proof of concept experiments show better OCF performance with pretrained encoder after JEPa-based world model learning.

1 INTRODUCTION

World models are becoming an increasingly important direction for autonomous driving, as they enable the prediction of spatial and temporal scenes, allowing vehicles to drive in imaginary space and simulate the future. Currently, most driving world models Hu et al. (2023a); Russell et al. (2025) are generative world models that explicitly generate pixel-level details for predicted future frames. However, this approach is computationally expensive to train and may suffer from hallucinations, producing physically implausible and inconsistent videos. On the other hand, some world models predict future states in latent space instead Li et al. (2024a); Zheng et al. (2025), which shows promise in terms of computational efficiency while ignoring certain pixel-level details.

However, representation collapse is a challenge in training latent world models, where all representations produced by the encoder collapse to constant vectors. LAW Li et al. (2024a) mitigates this issue by introducing an additional future waypoint regression loss, supervised by human drivers' waypoints, alongside the latent prediction loss. Such waypoints are often noisy, may be suboptimal, and in real-world scenarios may admit multiple plausible futures. Therefore, this training strategy may limit the expressiveness of the encoder's representations. In contrast, World4Drive Zheng et al. (2025) avoids representation collapse by utilizing auxiliary pretrained encoders, which require labeled data for training and thus limit scalability.

In this paper, we present **AD-LiST-JEPa** (Autonomous Driving with LiDAR data in a SpatioTemporal setting via Joint Embedding Predictive Architecture LeCun (2022)). JEPa is a paradigm that learns world models entirely in latent space without representation collapse, either by using a moving-average update of the target encoder or by maximizing the information captured by the encoder through explicit regularization, such as variance regularization. Previous work, AD-L-JEPa Zhu et al. (2025), explores JEPa for self-supervised representation learning in an autonomous driving single-frame LiDAR setting. AD-LiST-JEPa pushes this further by learning a latent world model that predicts future spatiotemporal representations from multi-frame LiDAR data.

2 RELATED WORKS

2.1 JEPA-BASED WORLD MODELS

World Models aim to predict the spatiotemporal evolution of an environment. At a high level, world models can be classified into *generative world models* Bruce et al. (2024); Hu et al. (2023a), which generate pixel-level details of predictions, and *non-generative world models*, which predict future representations at the latent level, e.g., *joint-embedding predictive architectures (JEPA)* LeCun (2022). World models based on JEPA propose predicting embeddings of masked or future image patches in a self-supervised manner Bardes et al. (2024) to capture multiple possible future states, rather than explicitly predicting data in pixel space. Recently, JEPA has been applied across different modalities, such as images Assran et al. (2023) and videos Bardes et al. (2024); Assran et al. (2025). In the context of autonomous driving, Zhu et al. (2025) explores LiDAR-based data in single-frame settings and evaluates the representation quality on a downstream LiDAR-based 3D object detection task. JEPA has shown promising results in leveraging world models for planning Zhou et al. (2024); Sobal et al. (2025).

2.2 LiDAR-BASED FUTURE FORECASTING TASKS

LiDAR is a key sensor in autonomous driving. Unlike camera images, LiDAR data are represented as sparse point clouds. To evaluate LiDAR-based world models, common downstream tasks include point cloud forecasting, occupancy forecasting, and occupancy completion (OCF). Point cloud forecasting directly predicts future point clouds, but as point clouds are strongly correlated with LiDAR sampling patterns (ray casting) and sensor intrinsics Khurana et al. (2023). Occupancy forecasting Khurana et al. (2023); Agro et al. (2024) mitigates this issue by predicting occupancy in a fixed-range bird’s-eye-view (BEV) grid or 3D voxel space, where a cell is considered occupied if it contains at least one point. Due to sparsity and occlusions, occupancy forecasting captures only partial object geometry. OCF Liu et al. (2024) extends occupancy forecasting by temporally aggregating points from the same instance over a long horizon, producing more complete occupancy labels. The downstream task is to predict this completed occupancy over time. As OCF evaluates both perception and prediction while providing more reliable scene geometry, we adopt it as a downstream task to assess world model capability in this paper.

3 METHOD

We propose a simple framework for self-supervised JEPA world model pretraining and supervised downstream OCF fine-tuning to evaluate the capability of world models. The framework consists of two phases: (1) self-supervised world modeling and (2) supervised downstream OCF finetuning. After Phase 1, we evaluate the JEPA-based world models by reusing the pretrained encoder for Phase 2 fine-tuning.

3.1 PHASE 1: SELF-SUPERVISED WORLD MODELING

The design philosophy is to train the network to predict the embeddings of masked multi-frame point cloud regions given the unmasked multi-frame point cloud regions, in order to capture the spatio-temporal evolution of the environment. To enable learning better representations, the novelty of our method lies in proposing a group BEV-guided masking strategy across frames that separates the ego vehicle from the world for JEPA training.

3.1.1 GROUP BEV-GUIDED MASKING

For the masking, on the one hand, the data collected at each time frame consist of ego-centric point clouds, which reflect both the evolution of the environment and the transformation of the ego vehicle from one frame to the next. These ego-motion transformations are recorded and known by the autonomous driving system Khurana et al. (2023). Therefore, to learn better representations, the ego vehicle should be separated from the world Sobal et al. (2022). On the other hand, if we directly extend AD-L-JEPA’s single-frame modified BEV-guided masking Zhu et al. (2025); Lin et al. (2022), which creates masks at BEV grids for both empty and non-empty cells, to multi-frame settings by propagating masks at the same spatial grid across time in ego-centric point clouds, the

motion of the ego vehicle will cause information leakage across time steps. To address this issue, we propose transforming each point p_j in the multi-frame data from time $-T$ to T into a common coordinate system at time 0 using the transformation $p'_j \leftarrow R^T p_j + c$, where R is the rotation matrix and c is the translation matrix.

After the coordinate transformation, another challenge in multi-frame LiDAR data is that the number of non-empty grids (i.e., grids that contain points) may vary across frames, even for the same spatial location. Therefore, we propose a group masking strategy across all frames. Specifically, we first map all points from all frames to spatial grids to determine whether each grid is empty or non-empty at the group level. We then propagate this group masking to each individual frame. For any grid that is non-empty in the group masking (i.e., contains an object across time) but is empty (caused by occlusion) in a particular frame, the masking state of that grid in that frame is determined by the group masking, while the grid itself is still treated as empty in that frame. The visualization of the proposed group masking is in Figure 1.

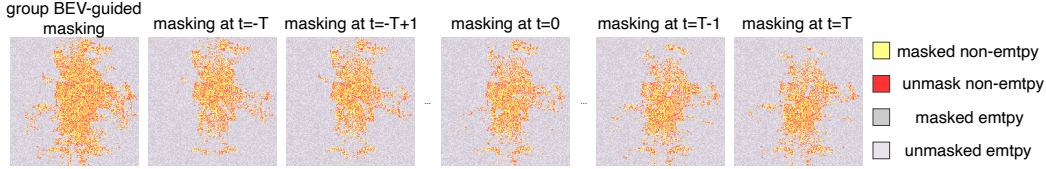


Figure 1: Proposed group BEV-guided masking.

3.1.2 NETWRK ARCHITECTURE

The architecture used in Phase 1 is inherited and adapted from AD-L-JEPA Zhu et al. (2025), which is designed for single-frame JEPA-based LiDAR representation learning. Notably, the context encoder and the backbone of the target encoder are identical to those of the single-frame sparse 3D convolutional network used in AD-L-JEPA. This design choice is intentional because, in autonomous driving settings, computational resources are limited. As a result, most existing state-of-the-art architectures Hu et al. (2023b); Li et al. (2024b) employ single-frame encoders rather than multi-frame encoders and aggregate features after independently encoding each frame. The key difference in our approach is that the input point clouds are multi-frame rather than single-frame. Masking is performed at the BEV grid level using our proposed group BEV-guided masking strategy and then upsampled back to the original point cloud to form multi-frame context and target point clouds. We reshape the output 3D voxel representations of each frame into per-frame BEV representations and concatenate them along the height dimension to obtain multi-frame BEV representations. Finally, a simple 3D convolutional predictor is applied to predict the target multi-frame BEV representations.

The loss consists of an embedding prediction loss and a regularization loss at non-empty grids:

$$\mathcal{L} = \mathcal{L}_{\text{jepa}} + \lambda_{\text{reg}} \mathcal{L}_{\text{reg}}, \quad (1)$$

Specifically, mask tokens and empty tokens are used to represent masked regions and empty-region embeddings, respectively, which is the same as that used in AD-L-JEPA Zhu et al. (2025). The pre-training objective includes a cosine-similarity-based embedding prediction loss applied to masked grids, along with a variance regularization loss applied to non-empty grids at the outputs of both the encoder and the predictor. We also experimented with SIGReg Balestriero & LeCun (2025) as the regularization loss. In this setting, no moving-average update is required: the context encoder and the target encoder are identical. SIGReg is applied to the outputs of both encoders, and the prediction loss is the L2 distance rather than cosine similarity. An overview of the network architecture variants during phase 1 is shown in Figure 3.1.2.

3.2 PHASE 2: EVALUATING WORLD MODELS WITH OCF FINETUNING

We evaluate world model representations on a downstream OCF task that captures dense scene geometry across frames. A sparse 3D encoder pretrained in Phase 1 extracts per-frame BEV features, which are concatenated into multi-frame representations. To assess the JEPA encoder’s representation quality, we keep the decoder as simple as possible by using a lightweight decoder with three

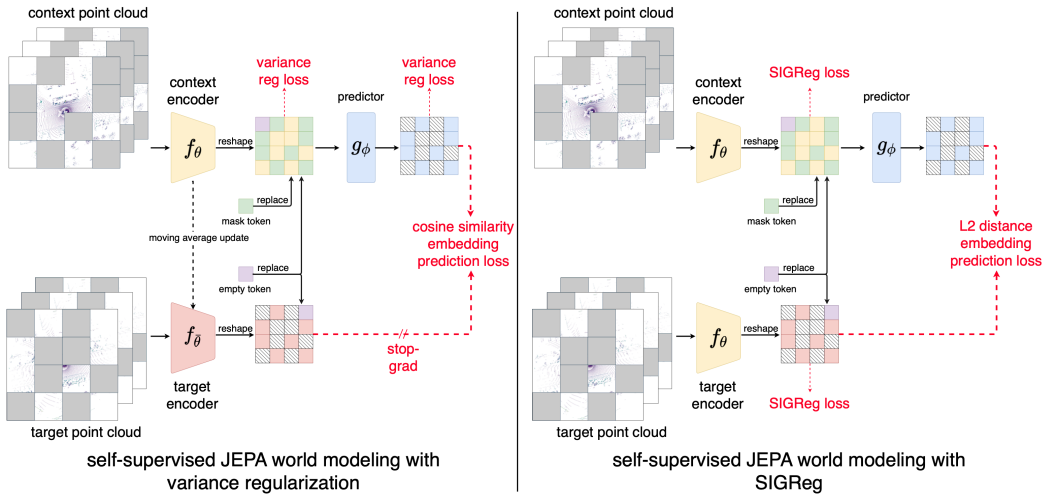


Figure 2: Overview of the Phase 1 framework with variance regularization (left) and SIGReg regularization (right) variants (best viewed when zoomed in).

convolutional layers to predict future BEV features, followed by a linear layer for per-grid binary classification and interpolation to the target OCF resolution. The model is trained with binary cross-entropy loss.

4 EXPERIMENTS

We use Waymo dataset Sun et al. (2020) for all experiments with OpenPCDet framework for LiDAR. Details on obtaining the training labels are provided in the supplementary materials as an extended explanation of the original paper Liu et al. (2024). We conduct Phase 1 pretraining for 30 epochs using 8 A100 GPUs with the Adam optimizer and a one-cycle learning rate scheduler, with a learning rate of 0.0003 and a weight decay of 0.01. For the variance regularization setting, we use a total batch size of 32, with the other hyperparameters set to the default values of AD-L-JEPA Zhu et al. (2025). For SIGReg, we train for 30 epochs using 8 A100 GPUs with a total batch size of 16; $\lambda_{\text{reg}} = 10$ for variance regularization and $\lambda_{\text{reg}} = 0.001$ for SIGReg. The masking ratio is set to 50% for non-empty grids and 50% for empty grids. For Phase 2 fine-tuning, we use a single A100 GPU with a batch size of 4 and a constant learning rate of 0.0005, and fine-tune the model for 3 epochs to predict the next 5 frames’ OCF label given the past 5 frames’ sparse input. For each fine-tuning run, we use three random seeds and report the mean and standard deviation in Table 4. The results show that the pretrained encoder of AD-LiST-JEPA outperforms training from scratch. Furthermore, the recently proposed SIGReg 2025 significantly outperforms variance regularization loss for this simple network architecture designed for the downstream task, indicating a promising direction for purely regularization-based methods to avoid representation collapse.

Method	IoU _{full} (%)	IoU _{close} (%)
scratch, linear	38.56 ± 0.19	42.87 ± 0.17
AD-LiST-JEPA, small	39.09 ± 0.36	43.43 ± 0.39
AD-LiST-JEPA, small, SIGReg	39.35 ± 0.24	43.70 ± 0.24
AD-LiST-JEPA, full	39.01 ± 0.47	43.46 ± 0.44
AD-LiST-JEPA, full, SIGReg	39.41 ± 0.31	43.86 ± 0.30

Table 1: Occupancy completion and forecasting segmentation performance on the Waymo dataset. “Small” and “large” denote Phase 1 pretraining with 190 and 950 Waymo sequences, respectively. IoU_{full} (%) is computed over the full range, while IoU_{close} is computed over a closer region with half the spatial extent in both x and y .

5 CONCLUSION

This paper presents a proof of concept for training JEPA-based spatiotemporal world models on multi-frame LiDAR data for autonomous driving. We evaluate the quality of the learned world models using a downstream occupancy completion and forecasting task. Our results indicate promising directions for future research; experiments on larger datasets and with larger network architectures will be explored in future work.

REFERENCES

Ben Agro, Quinlan Sykora, Sergio Casas, Thomas Gilles, and Raquel Urtasun. Uno: Unsupervised occupancy fields for perception and forecasting. In *Proceedings of the IEEE/CVF Conference on Computer Vision and Pattern Recognition*, pp. 14487–14496, 2024.

Mahmoud Assran, Quentin Duval, Ishan Misra, Piotr Bojanowski, Pascal Vincent, Michael Rabbat, Yann LeCun, and Nicolas Ballas. Self-supervised learning from images with a joint-embedding predictive architecture. In *Proceedings of the IEEE/CVF Conference on Computer Vision and Pattern Recognition*, pp. 15619–15629, 2023.

Mido Assran, Adrien Bardes, David Fan, Quentin Garrido, Russell Howes, Matthew Muckley, Ammar Rizvi, Claire Roberts, Koustuv Sinha, Artem Zhulus, et al. V-jepa 2: Self-supervised video models enable understanding, prediction and planning. *arXiv preprint arXiv:2506.09985*, 2025.

Randall Balestrieri and Yann LeCun. Lejepa: Provable and scalable self-supervised learning without the heuristics. *arXiv preprint arXiv:2511.08544*, 2025.

Adrien Bardes, Quentin Garrido, Jean Ponce, Xinlei Chen, Michael Rabbat, Yann LeCun, Mahmoud Assran, and Nicolas Ballas. Revisiting feature prediction for learning visual representations from video. *arXiv preprint arXiv:2404.08471*, 2024.

Jake Bruce, Michael D Dennis, Ashley Edwards, Jack Parker-Holder, Yuge Shi, Edward Hughes, Matthew Lai, Aditi Mavalankar, Richie Steigerwald, Chris Apps, et al. Genie: Generative interactive environments. In *Forty-first International Conference on Machine Learning*, 2024.

Anthony Hu, Lloyd Russell, Hudson Yeo, Zak Murez, George Fedoseev, Alex Kendall, Jamie Shotton, and Gianluca Corrado. Gaia-1: A generative world model for autonomous driving. *arXiv preprint arXiv:2309.17080*, 2023a.

Yihan Hu, Jiazhi Yang, Li Chen, Keyu Li, Chonghao Sima, Xizhou Zhu, Sqi Chai, Senyao Du, Tianwei Lin, Wenhui Wang, et al. Planning-oriented autonomous driving. In *Proceedings of the IEEE/CVF conference on computer vision and pattern recognition*, pp. 17853–17862, 2023b.

Wolfgang Kabsch. A solution for the best rotation to relate two sets of vectors. *Foundations of Crystallography*, 32(5):922–923, 1976.

Tarasha Khurana, Peiyun Hu, David Held, and Deva Ramanan. Point cloud forecasting as a proxy for 4d occupancy forecasting. In *Proceedings of the IEEE/CVF Conference on Computer Vision and Pattern Recognition*, pp. 11116–11124, 2023.

Yann LeCun. A path towards autonomous machine intelligence version 0.9. 2, 2022-06-27. *Open Review*, 62, 2022.

Yingyan Li, Lue Fan, Jiawei He, Yuqi Wang, Yuntao Chen, Zhaoxiang Zhang, and Tieniu Tan. Enhancing end-to-end autonomous driving with latent world model. *arXiv preprint arXiv:2406.08481*, 2024a.

Zhenxin Li, Kailin Li, Shihao Wang, Shiyi Lan, Zhiding Yu, Yishen Ji, Zhiqi Li, Ziyue Zhu, Jan Kautz, Zuxuan Wu, et al. Hydra-mdp: End-to-end multimodal planning with multi-target hydra-distillation. *arXiv preprint arXiv:2406.06978*, 2024b.

Zhiwei Lin, Yongtao Wang, Shengxiang Qi, Nan Dong, and Ming-Hsuan Yang. Bev-mae: Bird’s eye view masked autoencoders for point cloud pre-training in autonomous driving scenarios. *arXiv preprint arXiv:2212.05758*, 2022.

Xinhao Liu, Moonjun Gong, Qi Fang, Haoyu Xie, Yiming Li, Hang Zhao, and Chen Feng. Lidar-based 4d occupancy completion and forecasting. In *2024 IEEE/RSJ International Conference on Intelligent Robots and Systems (IROS)*, pp. 11102–11109. IEEE, 2024.

Lloyd Russell, Anthony Hu, Lorenzo Bertoni, George Fedoseev, Jamie Shotton, Elahe Arani, and Gianluca Corrado. Gaia-2: A controllable multi-view generative world model for autonomous driving. *arXiv preprint arXiv:2503.20523*, 2025.

Vlad Sobal, Alfredo Canziani, Nicolas Carion, Kyunghyun Cho, and Yann LeCun. Separating the world and ego models for self-driving. *arXiv preprint arXiv:2204.07184*, 2022.

Vlad Sobal, Wancong Zhang, Kyunghyun Cho, Randall Balestrieri, Tim GJ Rudner, and Yann LeCun. Learning from reward-free offline data: A case for planning with latent dynamics models. *arXiv preprint arXiv:2502.14819*, 2025.

Pei Sun, Henrik Kretzschmar, Xerxes Dotiwalla, Aurelien Chouard, Vijaysai Patnaik, Paul Tsui, James Guo, Yin Zhou, Yuning Chai, Benjamin Caine, et al. Scalability in perception for autonomous driving: Waymo open dataset. In *Proceedings of the IEEE/CVF conference on computer vision and pattern recognition*, pp. 2446–2454, 2020.

Yupeng Zheng, Pengxuan Yang, Zebin Xing, Qichao Zhang, Yuhang Zheng, Yinfeng Gao, Pengfei Li, Teng Zhang, Zhongpu Xia, Peng Jia, et al. World4drive: End-to-end autonomous driving via intention-aware physical latent world model. In *Proceedings of the IEEE/CVF International Conference on Computer Vision*, pp. 28632–28642, 2025.

Gaoyue Zhou, Hengkai Pan, Yann LeCun, and Lerrel Pinto. Dino-wm: World models on pre-trained visual features enable zero-shot planning. *arXiv preprint arXiv:2411.04983*, 2024.

Haoran Zhu, Zhenyuan Dong, Kristi Topollai, and Anna Choromanska. Ad-l-jepa: Self-supervised spatial world models with joint embedding predictive architecture for autonomous driving with lidar data. *arXiv preprint arXiv:2501.04969*, 2025.

A APPENDIX

This part is not novel; it is an extended description of the data processing pipeline in Liu et al. (2024), with pseudocode to help readers better understand the data processing pipeline. The visualization of past raw input point clouds is shown in Figure A, while the future completed occupancy ground-truth labels after data processing are visualized in Figure A.

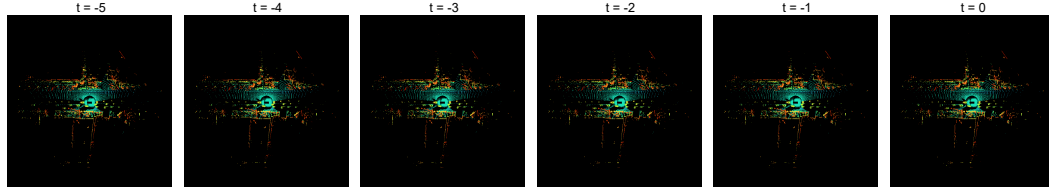


Figure 3: Raw past (including current) point cloud visualization as the neural network input from time -5 to 0. The color represents height relative to the ground.

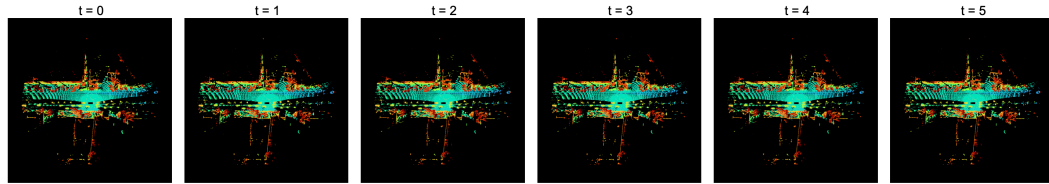


Figure 4: Processed future (including current) completed occupancy visualization as the neural network prediction target from time 0 to 5. The color represents height relative to the ground.

The data processing contains two phase:

- LiDAR sequence transformation
- voxelization with ray casting

A.1 LiDAR SEQUENCE TRANSFORMATION

The ultimate goal of this component is to aggregate points belonging to the same object instance across previous and subsequent frames. First, a coordinate transformation is applied to map ego-centric points into a unified reference coordinate system at the current time step. This process includes ghost object removal, which eliminates objects that appear in previous or subsequent frames but are absent in the current frame, as well as moving object alignment for objects present in the current frame. Points from these objects are then aggregated using instance bounding boxes from other frames. Singular Value Decomposition (SVD) is used to solve the orthogonal Procrustes problem for this aggregation Kabsch (1976). The algorithm is summarized in Algorithm 1.

A.2 VOXELIZATION WITH RAY CASTING

After Algorithm 1, a densified point cloud is obtained by aggregating instances across time. To generate the completed occupancy, voxelization with ray casting is then applied. Rays are cast from the origin to each point to determine whether voxels along each ray are occupied (contain points), empty (contain no points), or invalid (no rays pass through them). The resulting occupancy and invalid masks are used for network training and evaluation. The algorithm is summarized in Algorithm 2.

Algorithm 1 LiDAR Sequence Transformation

```
1: procedure TRANSFORM(idcur)
2:    $L \leftarrow$  total length of the sequence
3:    $p_{\text{dict}}^{\text{cur}} \leftarrow \{\}$ 
4:   for each frame  $i \leftarrow \text{id}_{\text{start}}$  to  $\text{id}_{\text{end}}$  and  $i \neq \text{id}_{\text{cur}}$  do
5:      $\text{pose}_i \in \mathbb{R}^{4 \times 4} \leftarrow$  pose at time index  $i$ 
6:      $B_{\text{cur}} \leftarrow$  instance boxes at time  $\text{id}_{\text{cur}}$ 
7:      $B_i \leftarrow$  instance boxes at time  $i$ 
8:     for each instance box  $j \leftarrow 0$  to  $|B_i| - 1$  do
9:       if  $B_i[j] \notin B_{\text{cur}}$  then
10:         delete points for instance  $j$  at time  $i$ 
11:       else if  $B_i[j] \in B_{\text{cur}}$  then
12:          $m \leftarrow$  index of the same instance in  $B_{\text{cur}}$ 
13:          $(R, c) \leftarrow \text{SVD\_Align}(B_i[j], B_{\text{cur}}[m])$ 
14:          $p_j \leftarrow$  points of in  $B_i[j]$ 
15:          $T_{\text{cur}}^{\text{global}} \leftarrow$  current to global pose
16:          $T_i^{\text{global}} \leftarrow$  time  $i$  to global pose
17:          $\tilde{p}_j = \{T_i^{\text{global}}\}^{-1} T_{\text{cur}}^{\text{global}} \begin{bmatrix} R^T p_j + c \\ \mathbf{1} \end{bmatrix}$ 
18:         replace  $p_j$  with  $\tilde{p}_j$  for points at frame  $i$ 
19:       end if
20:     end for
21:      $p_{\text{dict}}^{\text{cur}}[i] \leftarrow$  updated points at frame  $i$ 
22:   end for
23:   return  $p_{\text{dict}}^{\text{cur}}$ 
24: end procedure
```

Algorithm 2 Obtain Network Input and Outputs

```

1: procedure TRANSFORM(idcur)
2:    $L \leftarrow$  total length of the sequence
3:    $R \leftarrow (x_{\min}, y_{\min}, z_{\min}, x_{\max}, y_{\max}, z_{\max})$ , range
4:    $V \leftarrow (v_x^{\text{size}}, v_y^{\text{size}}, v_z^{\text{size}})$ , voxel size
5:    $\tilde{O}^{\text{sparse.input}} = []$ 
6:   for each frame  $i \leftarrow id_{\text{cur}} - N_{\text{pre}}$  to  $id_{\text{cur}}$  do
7:      $P_i^{\text{all}} \leftarrow$  all points at time i
8:      $T_i^{\text{global}} \leftarrow$  time i to global pose
9:      $\tilde{P}_i^{\text{all}} \leftarrow \{T_{\text{cur}}^{\text{global}}\}^{-1} T_i^{\text{global}} P_i^{\text{all}}$ 
10:     $q_i^{\text{origin}} \leftarrow$  sensor origin at time i
11:     $O_i^{\text{sparse.occ}}, - \leftarrow \text{RayCast}(q_i, \tilde{P}_i^{\text{all}}, R, V)$ 
12:     $\tilde{O}^{\text{sparse.input}}.append(\tilde{P}_i^{\text{all}})$ 
13:   end for
14:
15:    $O^{\text{occ}} = []$ 
16:    $O^{\text{invalid}} = []$ 
17:   for each frame  $i \leftarrow id_{\text{cur}}$  to  $id_{\text{cur}} + N_{\text{post}}$  do
18:      $T_i^{\text{global}} \leftarrow$  time i to global pose
19:      $K_{\text{start}} \leftarrow \max(i - N_{\text{pre}}, 0)$ 
20:      $K_{\text{end}} \leftarrow \min(i + N_{\text{post}}, L)$ 
21:      $P_i^{\text{aggr}} \leftarrow []$ 
22:     for each frame  $j \leftarrow K_{\text{start}}$  to  $K_{\text{end}}$  do
23:        $P_j^{\text{all}} \leftarrow$  all points at time j
24:        $T_j^{\text{global}} \leftarrow$  time j to global pose
25:        $\tilde{P}_j^{\text{all}} \leftarrow \{T_{\text{cur}}^{\text{global}}\}^{-1} T_j^{\text{global}} P_j^{\text{all}}$ 
26:        $P_i^{\text{aggr}}.append(\tilde{P}_j^{\text{all}})$ 
27:     end for
28:      $q_i^{\text{origin}} \leftarrow$  sensor origin at time i
29:      $O_i^{\text{occ}}, O_i^{\text{invalid}} \leftarrow \text{RayCast}(q_i^{\text{origin}}, P_i^{\text{aggr}}, R, V)$ 
30:      $O^{\text{occ}}.append(O_i^{\text{occ}})$ 
31:      $O^{\text{invalid}}.append(O_i^{\text{invalid}})$ 
32:   end for
33:   return  $(\tilde{O}^{\text{sparse.input}}, O^{\text{occ}}, O^{\text{invalid}})$ 
34: end procedure

```
